Cerebral Cortex, August 2018;28: 2786–2794

doi: 10.1093/cercor/bhx158
Advance Access Publication Date: 24 June 2017
Original Article

ORIGINAL ARTICLE

Neuromodulation of Axon Terminals

Darpan Chakraborty[1], Dennis Q. Truong[2], Marom Bikson[2] and Hanoch Kaphzan[1]

[1]Sagol Department of Neurobiology, University of Haifa, Haifa 3498838, Israel and [2]Department of Biomedical Engineering, The City College of New York of CUNY, New York, NY 10031, USA

Address correspondence to Dr Hanoch Kaphzan, Sagol Department of Neurobiology, University of Haifa, 199 Aba Khoushy Avenue, Mt. Carmel, Haifa 3498838, Israel. Email: hkaphzan@univ.haifa.ac.il

Abstract

Understanding which cellular compartments are influenced during neuromodulation underpins any rational effort to explain and optimize outcomes. Axon terminals have long been speculated to be sensitive to polarization, but experimentally informed models for CNS stimulation are lacking. We conducted simultaneous intracellular recording from the neuron soma and axon terminal (blebs) during extracellular stimulation with weak sustained (DC) uniform electric fields in mouse cortical slices. Use of weak direct current stimulation (DCS) allowed isolation and quantification of changes in axon terminal biophysics, relevant to both suprathreshold (e.g., deep brain stimulation, spinal cord stimulation, and transcranial magnetic stimulation) and subthreshold (e.g., transcranial DCS and transcranial alternating current stimulation) neuromodulation approaches. Axon terminals polarized with sensitivity (mV of membrane polarization per V/m electric field) 4 times than somas. Even weak polarization (<2 mV) of axon terminals significantly changes action potential dynamics (including amplitude, duration, conduction velocity) in response to an intracellular pulse. Regarding a cellular theory of neuromodulation, we explain how suprathreshold CNS stimulation activates the action potential at terminals while subthreshold approaches modulate synaptic efficacy through axon terminal polarization. We demonstrate that by virtue of axon polarization and resulting changes in action potential dynamics, neuromodulation can influence analog–digital information processing.

Key words: action potential properties, analogue–digital information processing, axon bleb, membrane polarization modeling, threshold latency

Introduction

Electrical neuromodulation of the CNS can produce behavioral and clinical changes (Antal et al. 2014), as a complementary treatment strategy to pharmacological approaches. Understanding the cellular targets of neuromodulation, namely, which neuronal compartments are activated during stimulation, is the fundamental building block of mechanistic understanding and rational technique optimization (Rattay 1999). Stimulation of axons (including terminals) has been indirectly implicated in neuromodulation approaches spanning from deep brain stimulation (DBS) (McIntyre et al. 2004), spinal cord stimulation (SCS) (Holsheimer 2002), transcranial magnetic stimulation (TMS); (Pashut et al. 2011; Salvador et al. 2011), to transcranial direct current stimulation (tDCS) (Rahman et al. 2013). Indeed, for decades, axon terminals have been theoretically speculated to be the most sensitive compartments to electrical stimulation (Ranck 1975; Tranchina and Nicholson 1986; Nowak and Bullier 1998; Arlotti et al. 2012).

Modern neurophysiology reinforces the importance of the axon for CNS information processing. Relevant for suprathreshold stimulation, the action potential (AP) is generated at the distal portion of the axon initial segment (Palmer and Stuart 2006; Kole et al. 2007; Shu et al. 2007; Kole and Stuart 2008, 2012). Previously, APs were considered as the all-or-none digital signals which are simply converted by neurons from incoming inputs to outputs. However, modern neurophysiology has

identified a role for analog AP conduction. The AP is sensitive to a weak subthreshold polarization of the axonal membrane, which subsequently induces a modification in the shape of the AP (Bischofberger et al. 2006; Shu et al. 2006). Broader or narrower APs can, respectively, cause prolonged or abbreviated terminal polarization, and it is well established that neurotransmitter release is sensitive to terminal polarization (Shu et al. 2006; Kole et al. 2007; Debanne et al. 2011). Thus, the primary digital information that is presynaptic activity is preserved, but the analog content that is membrane potential modifies the weight of the hybrid signal which allows far more information to be contained in a single AP compared with conventional digital signaling (Stuart and Sakmann 1994; Clark and Häusser 2006). Therefore, we propose that the concept of analog signal transfer suggests a novel mechanism for electrical stimulation of axons, especially subthreshold stimulation.

This report is the first direct recording from mammalian axons during extracellular electrical stimulation. We conducted simultaneous intracellular recording from the somas and axon terminals (blebs) of single neurons. To develop a quantitative model of axon terminal neuromodulation (e.g., coupling constants), we applied sustained (direct current) low-intensity, uniform electric fields (EFs), (Bikson et al. 2004; Radman et al. 2009) and assessed changes in passive and active/dynamic properties. The resulting quantitative model can be applied to any method of neuromodulation including suprathreshold (DBS, SCS, and TMS) and subthreshold (tDCS) approaches. In addition, emerging evidence in neuroscience indicates that axonal AP initiation and conduction is not a simple digital function but entail analog properties as well (Alle and Geiger 2006). Our results are the first to indicate that brain stimulation modulates the analog mode of signal transduction and conduction velocity of already generated APs, and further suggest a role of neuromodulation in signal synchrony.

Methods

Subjects and Slice Preparations

All experimental procedures were performed in accordance with National Institutes of Health guidelines and were approved by the University of Haifa animal ethics committee. In total 51 C57BL/6 mice of either sex were sacrificed by cervical dislocation and brains were quickly removed and coronal prefrontal cortical slices (300 μm) were isolated with a Campden Vibratome 7000 smz2 (Campden Instruments, UK) in ice-cold cutting solution (in mM): 110 sucrose, 60 NaCl, 3 KCl, 1.25 NaH_2PO_4, 28 $NaHCO_3$, 0.5 $CaCl_2$, 7 $MgCl_2$, 5 glucose. Slices were recovered for 45 min at 36°C in artificial cerebrospinal fluid (ACSF) containing in mM: 125 NaCl, 2.5 KCl, 1.25 NaH_2PO_4, 25 $NaHCO_3$, 25 D-glucose, 2 $CaCl_2$, and 1 $MgCl_2$ ACSF, followed by additional recovery for 30 min in room temperature ACSF. After initial recovery, slices were placed in a submerged chamber and maintained at room temperature in ACSF (2 mL/min).

Whole-Cell Recording

Slices recovered for an additional 60 min on the electrophysiology rig, before experimentation. All solutions were constantly caboxygenated with 95% O_2 + 5% CO_2. Cortical regions of brain slices were illuminated and visualized using an x60 water-immersion objective mounted on a fixed-stage microscope (BX51-WI, Olympus, Center Valley, PA), and the image was displayed on a video monitor using a charge-coupled device camera IR-1000 (Dage MTI, Michigan City, IN). Recordings were amplified by multiclamp 700B and digitized by Digidata 1440 (molecular devices, Sunnyvale, CA). Whole-cell recordings were performed as described previously (Kaphzan et al. 2013). A custom apparatus was prepared to combine dual patch of the soma and the axon bleb, as outlined in the literature (Fig. 1*a*) (Shu et al. 2006; Hu and Shu 2012). The uniform DC EF was generated by linear stimulus isolation unit (LSIU-02, Cygnus Technology, PA, USA) and the cathode and anode were custom made with $AgCl_2$ covered silver wires (783500, AM-System, WA, USA). The applied current was adjusted for each experiment (ranging from 58.3 to 34.8 μA), and resultant uniform EF of 5 V/m was precisely delivered and monitored throughout the experiment (Bikson et al. 2004). Borosilicate glass pipettes (3–5 MΩ for soma, 7–9 MΩ for axon) were pulled (P-1000; Sutter Instruments, Navato, CA) and filled with a K-gluconate based internal solution (in mM): 120K-gluconate, 20 KCl, 10 HEPES, 2 $MgCl_2$, 4 Na2ATP, 0.5 TrisGTP, 14 phosphocreatine, Alexa-488 (100 μM) osmolarity 290 mOsm and pH = 7.3. Pyramidal cells soma region at layer-5 were patched and allowed 10 min for the cells to be filled with the fluorescent dye (Fig. 1*c*), a brief fluorescence exposure (less than 20 s) allowing tracing of terminal bleb of the axon on the surface of the slice. The dendritic tree remains intact inside the slice (Fig. 1*d*). The alignment between the EF and the axon segment (Θ, Fig. 1*b* and Table S1.) was used to calculate the effective EF (EF·Cos Θ) and classify stimulation as parallel (Θ: −30 to 30) or orthogonal (Θ: 60–120) DCS. Polarization length/coupling constant (Radman et al. 2009) was calculated as membrane polarization per V/m of effective EF. Reversing the direction of the current application (5 V/m for 1 min) produced depolarized (dep) or hyperpolarized (hyp) DCS for both the parallel and orthogonal field orientations. Axonal polarization was determined by subtracting the change in axon bleb resting membrane potential from the change in somatic resting membrane potential. We corrected for alterations of external bath potentials by subtracting the respective voltage recorded by 2 extracellular reference electrodes proximal to each intracellular recording location, soma and bleb. The method for measuring active intrinsic properties from single AP was based on previous studies with 10 pA current injection steps for 10 ms in soma (Kaphzan et al. 2011, 2013). The first single AP at 5 ms from the start of the current injection was analyzed (Fig. S1a–c). Membrane potential acceleration to 30 V/s point determined AP threshold. All current-clamp recordings were low-pass filtered at 10 kHz and sampled at 50 kHz. Series resistance was compensated and only series resistance <15 MΩ for soma recording and <35 MΩ for axon recording were included in data set. Series resistance, input resistance, and membrane capacitance were monitored during the entire experiment. Changes of these parameters, from beginning to end of the experiment, >10% were criteria for the exclusion of data.

Statistical Analysis

The analysis was done with Clampfit 10 (Molecular Devices, Sunnyvale CA, USA) and SPSS 23 (IBM, Armonk NY, USA). One way and repeated measure ANOVA was used for electrophysiological data analysis with $P < 0.05$ as significance criteria Bonferroni in post hoc test.

Simulation and Modeling

A biophysical model of neuron polarization was implemented in NEURON (Hines and Carnevale 1997) including a dendritic, somatic, up to 400 μm axon, and a bleb compartment (Fig. 1*g*).

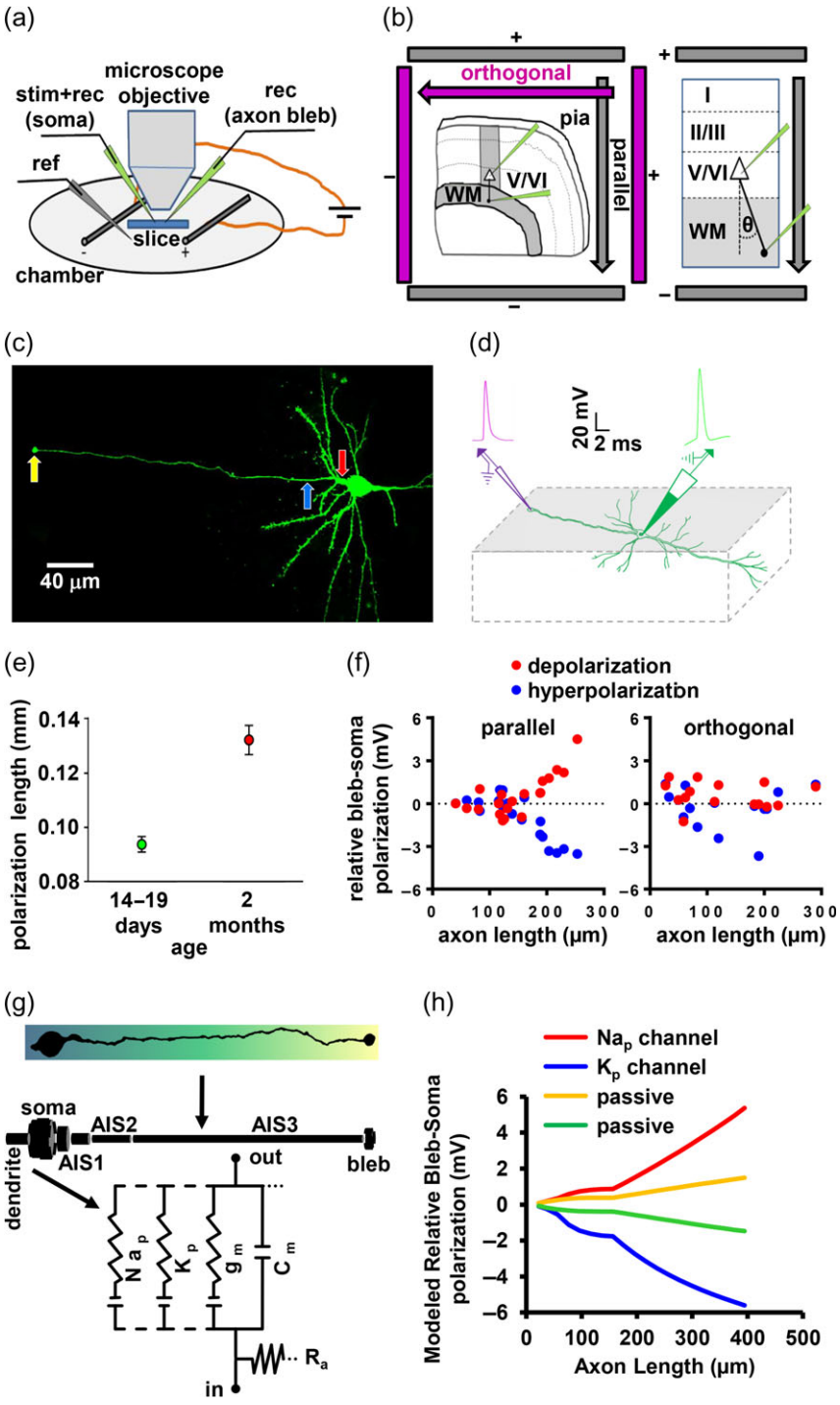

Figure 1. Recording set-up and passive property alterations in experimental and modeling results. Custom made experimental set-up with Ag-$AgCl_2$ electrodes producing uniform electric fields across the slice. Soma electrode stimulated and recorded the response, while the bleb electrode only recorded the respective response. The reference microelectrode used to measure the bath polarization (*a*). For parallel field stimulation, the electrodes were placed across the slice such that the electric field was parallel to the dendro-axonic axis of the layer-V pyramidal cells, whereas for the orthogonal orientation the electric field is perpendicular to the dendro-axonic axis (*b*, left). The axonal alignment, θ, relative to the electric field was determined for each cell (*b*, right). Sample image of a layer-V pyramidal cell, filled with Alexa-488 presented here (*c*). (red arrow: axon hillock, blue arrow: axon initial segment, yellow arrow: axon bleb). Cellular orientation in the slice is illustrated in the schematic (*d*). The axon bleb is patched at the surface of the slice whereas the dendrite remains intact deep inside the slice. Average polarization length of P14–19 ($N = 12$, $n = 250$) is significantly lower than in young adult (2 months) ($N = 5$, $n = 41$) (*e*). Relative bleb–soma polarization as a function of the axonal length (*f*). In the parallel orientation, the relative polarity-specific (dep and hyper) polarization was evident started only in the axons longer than 100 µm ($N = 19$, $n = 19$). In the orthogonal orientation, the relative polarization was not affected significantly ($N = 15$, $n = 15$). Compartmentalization of a neuron for the polarization modeling (*g*), where, AIS1 represents the axon hillock, AIS2 is the axon initial segment and AIS3 denotes the axon. Models of relative polarization predicted similar polarization as experimental data, but only when persistent sodium current (Na_p) and persistent potassium current (K_p) were considered in addition to the passive membrane properties (*h*). (Depolarized passive: yellow, hyperpolarized passive: green, depolarized active: red, hyperpolarized active: blue).

Axons of varying length were modeled and the relative bleb–soma polarization compared. Membrane and additional channel properties were adapted from literature (Migliore 1996; Bahl et al. 2012). For an active model, persistent sodium (Na_p) or persistent potassium (K_p) channels were added to the neuron terminal to mimic a nonlinear response to either depolarization or hyperpolarization.

Results

Polarization Length Alters With Age

Consistent with prior reports in other animal models (Radman et al. 2009; Fröhlich et al. 2010), the somas of pyramidal neurons polarized in response to parallel DCS in a polarity-specific manner; in adult animals (2 months old) we report comparable sensitivity 0.13 ± 0.01 mm [the values are mean ± standard error of the mean (SEM), ranging 0.06–0.18 mm] (Fig. 1*e*), while at younger ages (P14–19) we observed a reduced but significant polarization length 0.093 ± 0.003 mm (ranging 0.03–0.19 mm) (Fig. 1*e* and Fig. S3a). Axon blebs are a physical model of endogenous axon terminals, accessible with patch only in the absence of myelin (Hu and Shu 2012); remaining experiments were, therefore, performed in mice are in the early developmental stages (P14–19).

Axon Terminal Polarization Alterations With DCS

A dual patch of the soma and the axon bleb were recorded during DCS. To increase accuracy, axon bleb polarization during DCS was measured relative to the soma polarization with extracellular voltage deflections subtracted for each recording location (Radman et al. 2009; Fröhlich et al. 2010; Arlotti et al. 2012). Consistent with biophysical theory, the axon terminal polarization decoupled from soma polarization with increasing distance for axons longer than 100 μm (Fig. 1*f* and Fig. S2a,b) (McIntyre et al. 2004; Strüber et al. 2014). However, the relative bleb–soma polarization increased as a function of axon length faster than the maximum predicted for a passive model and was only approximated with an active model (Fig. 1*g*,*h*). Passive relative polarization as a function of axon length was limited by the rate of extracellular polarization (5 V/m). Parallel but not orthogonal directed stimulation was effective, with a maximum-recorded sensitivity of ~0.8 mm (Fig. 1*f*).

DCS Differentially Affects Active Intrinsic Properties in the Soma and Axon Bleb

Using intracellular current injection to probe passive and active neuron response, changes in the intrinsic properties under DCS application were analyzed for axon blebs >100 μm from the soma (to decouple from soma effects). In congruence with our polarization results, depolarizing and hyperpolarizing DCS, in parallel and orthogonal orientations, significantly affect active intrinsic properties only in the axon blebs but not in the somas (Table 1, and for sample traces Fig. S1d–g). Only at axon blebs, depolarizing parallel current induces a decrease of AP amplitude and maximal rate of rise, but an increase of AP midwidth with a net increase in area under the curve (AUC) (Table 1 and Fig. S1d–g). Relatively minor effects for orthogonal compared with parallel DCS, likely reflect minimally, but not zero, terminal polarization. Furthermore, for both depolarization and hyperpolarization parallel DCS; there was a linear correlation between the extent of change (ratios) in the AP amplitude and mid-width and the axon bleb distance (Fig. 2*a*–*h*). Consistent with the hypothesis that effects on AP dynamics are driven by the terminal polarization, modulation of AP amplitude and midwidth strongly correlated with terminal polarization by DCS (Fig. 2*I*,*j*). Threshold current injection to the soma, which induces firing in the axon initial segment, was reduced for depolarized parallel DCS, while AP threshold potential and input resistance as measured in the soma were not significantly changed (Table 1).

Distinctive Effect of Parallel and Orthogonal Field on Threshold Latency and AP Conduction Velocity

We defined the delay of threshold potential in the soma and the axon bleb, as threshold latencies. Longer the axon, higher the threshold latency (Fig. 3*a*). The correlation of threshold latencies to the axon bleb distance in the dep, hyp and without DCS show that the linear regression lines for all 3 conditions ($R^2 \approx 0.98$). Moreover, while the dissection point for latency = 0 is unaltered between the 3 conditions (~91 μm), the slope of linear regression lines are significantly different ($P < 0.0001$) (Fig. 3*b*,*c*). This is consistent with different conduction velocities between all the 3 conditions, while the triggering point probably is not significantly altered. DCS depolarization induces an increased conduction velocity, while DCS hyperpolarization reduces conduction velocity (repeated measures of ANOVA of velocities across the 3 conditions per axon bleb; $P < 0.0001$ for both) (Fig. 3*d*).

Discussion

For clinically established (FDA approved) neuromodulation techniques such as DBS, SCS, repetitive rTMS, and electroconvulsive therapy (ECT), quantifying the cellular targets of stimulation provides a substrate for ongoing optimization. For investigational techniques, such as tDCS, transcranial alternating current stimulation (tACS), and transcranial random noise stimulation (tRNS), a quantitative model of cellular targets also help establish plausible efficacy. The behavioral and clinical outcomes of these neuromodulation techniques are distinct and complex but are assumed to all derive from the generation of EFs in the brain, leading to the polarization of cells. It has long been speculated that the most sensitive cells to polarization are neurons by virtue of the extended axonal compartments, and extensive conceptual and therefore computational models have been developed around axon stimulation (Ranck 1975; Tranchina and Nicholson 1986; Nowak and Bullier 1998; Arlotti et al. 2012). However, until now evidence in humans (and animal models) was indirect; for example, observation that APs are initiated in cortical neurons at EF at amplitudes below stimulation intensities needed to polarize soma to firing (Radman et al. 2009), chronaxie analysis (Nowak and Bullier 1998), or that modulation of synaptic efficacy is consistent with expectations about terminal polarization (Purpura and McMurtry 1965; McIntyre et al. 2004; Kabakov et al. 2012; Márquez-Ruiz et al. 2012; Rahman et al. 2013). Here, we not only quantify the sensitivity of mammalian axons to electrical stimulation but further show how polarization changes terminal excitability. Moreover, orientations-specific effects of DCS on mammalian cortical excitability in vitro have been noted (Bikson et al. 2004; Kabakov et al. 2012; Rahman et al. 2013) and the present results shed new light on suggested underlying mechanisms.

The average soma polarization length for adult mice (0.13 mm) we report is comparable to findings in the other species (Radman et al. 2009; Fröhlich et al. 2010). We discovered

Table 1 AP properties in the parallel and orthogonal field for the axons longer than 100 μm

AP properties in axon bleb							
Orientation (N = mice, n = cells)	Field direction	Threshold potential (mV)	AP amplitude (mV)	AP mid-width (ms)	AP max dv/dt (V/s)	AP AUC (mV × ms)	
Parallel (N = 16, n = 16)	No	−51.62 ± 1.16	42.32 ± 2.28	2.44 ± 0.10	150.51 ± 16.13	154.46 ± 13.01	
	Hyp	−51.88 ± 0.86	47.35 ± 2.33***	2.20 ± 0.08***	156.85 ± 16.01***	149.38 ± 12.18**	
	Dep	−53.03 ± 0.92	37.70 ± 2.39***	2.67 ± 0.11***	145.81 ± 15.62***	162.13 ± 13.67**	
Orthogonal (N = 8, n = 8)	No	−49.54 ± 2.09	34.80 ± 1.19	1.96 ± 0.06	137.59 ± 10.90	154.47 ± 12.08	
	Hyp	−49.43 ± 2.35	37.73 ± 2.63*	1.89 ± 0.05	143.29 ± 11.33*	149.38 ± 13.80	
	Dep	−49.44 ± 2.20	31.92 ± 2.58*	2.07 ± 0.05	135.42 ± 11.11	158.15 ± 11.64	
F values	Direction	$F_{1.54,19.96} = 0.441$, $P = 0.598$	$F_{1.44,31.70} = 123.43$, $P < 0.001$	$F_{1.29,28.48} = 25.78$, $P < 0.001$	$F_{1.20,26.53} = 29.80$, $P < 0.001$	$F_{1.25,27.56} = 18.53$, $P < 0.001$	
	Orientation × direction	$F_{1.54,19.96} = 0.650$, $P = 0.494$	$F_{1.44,31.70} = 22.98$, $P < 0.001$	$F_{1.29,28.48} = 9.72$, $P = 0.002$	$F_{1.20,26.53} = 0.92$, $P = 0.366$	$F_{1.25,27.56} = 0.844$, $P = 0.437$	

AP properties in soma								
							Input resistance (MΩ)	Threshold current (pA)
Parallel (N = 16, n = 16)	No	−41.45 ± 1.39	84.55 ± 1.91	2.24 ± 0.06	180.84 ± 12.94	384.84 ± 9.92	76.12 ± 4.73	286.25 ± 7.46
	Hyp	−40.74 ± 1.53	84.27 ± 1.91	2.21 ± 0.06	182.75 ± 13.37	378.07 ± 11.39	75.38 ± 4.65	293.75 ± 7.2***
	Dep	−39.49 ± 1.61	83.22 ± 1.93	2.33 ± 0.08	180.17 ± 13.35	385.25 ± 9.91	85.38 ± 6.42	279.37 ± 7.39***
Orthogonal (N = 8, n = 8)	No	−42.38 ± 4.11	87.28 ± 2.85	1.92 ± 0.09	151.07 ± 16.08	286.91 ± 19.65	58.44 ± 6.69	300 ± 10.69
	Hyp	−40.99 ± 4.32	87.66 ± 2.79	1.88 ± 0.09	252.30 ± 15.95	285.73 ± 19.39	60.50 ± 6.57	302.5 ± 10.65
	Dep	−42.94 ± 4.37	86.98 ± 2.84	1.95 ± 0.08	250.24 ± 15.92	285.90 ± 19.82	56.42 ± 9.08	298.75 ± 11.56
F values	Direct	$F_{1.16,25.56} = 0.789$, $P = 0.401$	$F_{1.21,26.7} = 1.54$, $P = 0.231$	$F_{1.17,25.70} = 5.17$, $P = 0.027$	$F_{1.72,37.81} = 5.16$, $P = 0.02$	$F_{1.02,22.31} = 0.74$, $P = 0.401$	$F_{1.16,25.48} = 0.724$, $P = 0.422$	$F_{1.64,36.18} = 28.133$, $P < 0.001$
	Orient × direct	$F_{1.16,25.56} = 1.98$, $P = 0.171$	$F_{1.21,26.7} = 0.44$, $P = 0.551$	$F_{1.17,25.70} = 0.70$, $P = 0.431$	$F_{1.72,37.81} = 0.11$, $P = 0.87$	$F_{1.02,22.31} = 0.52$, $P = 0.483$	$F_{1.16,25.48} = 0.2.70$, $P = 0.109$	$F_{1.64,36.18} = 9.64$, $P = 0.001$

All analysis was done by repeated measure ANOVA, multiple comparisons Bonferroni corrections with $P < 0.05$ and the values in the table are mean ± SEM. The effect of the field always measured with respect to the no field.
*$P < 0.05$, **$P < 0.01$, ***$P < 0.001$.

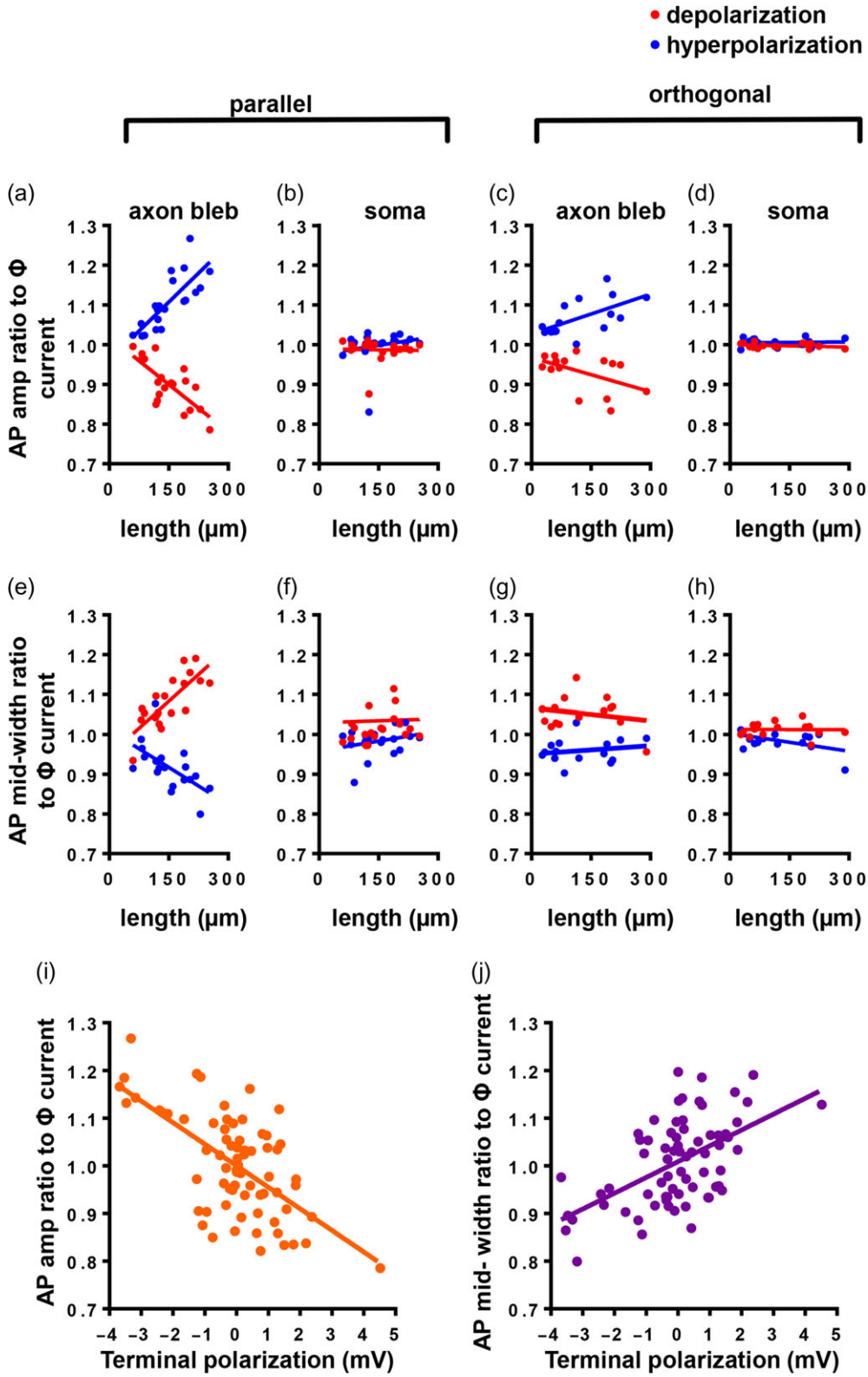

Figure 2. AP amplitude and midwidth ratio alterations to *Φ* change of current under parallel or orthogonal electric field. For parallel electric field orientation, the axonal AP amp ratio to *Φ* change of current is linearly correlated to axonal length for both depolarizing and hyperpolarizing polarities (*a*) (red, dep field, $R^2 = 0.53$, $P < 0.001$; blue, hyp field, $R^2 = 0.61$, $P < 0.0001$) while the soma is not affected (*b*) (red, dep field, $R^2 = 0.0008$, $P = 0.906$; blue, hyp field, $R^2 = 0.0414$, $P = 0.389$). For orthogonal electric field orientation axonal AP amplitude ratio to Φ change of current is linearly correlated to axonal length for hyperpolarizing polarity but not in depolarizing polarity (*c*) (red, dep field, $R^2 = 0.24$, $P = 0.062$; blue, hyp field, $R^2 = 0.34$, $P = 0.02$) with no effect at the soma (*d*) (red, dep field, $R^2 = 0.079$, $P = 0.3089$; blue, hyp field, $R^2 = 0.0034$, $P = 0.8359$). With parallel field orientation, AP mid-width ratio to Φ change of current also linearly correlates with the axonal length in axon (*e*) (red, dep field, $R^2 = 0.6$, $P < 0.0001$; blue, hyp field, $R^2 = 0.36$, $P < 0.0057$) but not in soma (*f*) (red, dep field, $R^2 = 0.0004$, $P = 0.9298$; blue, hyp field, $R^2 = 0.07097$, $P = 0.2562$). Whereas in the orthogonal field the ratio is not linearly correlated, neither in axon (*g*) (red, dep field, $R^2 = 0.04$, $P = 0.45$; blue, hyp field, $R^2 = 0.04$, $P = 0.5$) nor in soma (*h*) (red, dep field, $R^2 = 0.0001$, $P = 0.968$; blue, hyp field, $R^2 = 0.2263$, $P = 0.0731$). In parallel orientation AP amp ratio and mid-width ratio to Φ change of current are linearly correlated to terminal polarization, (*i*) ($R^2 = 0.3985$, $P < 0.0001$) and (*j*) ($R^2 = 0.3003$, $P < 0.0001$), respectively. (Parallel, $N = 19$, $n = 19$; orthogonal, $N = 15$, $n = 15$).

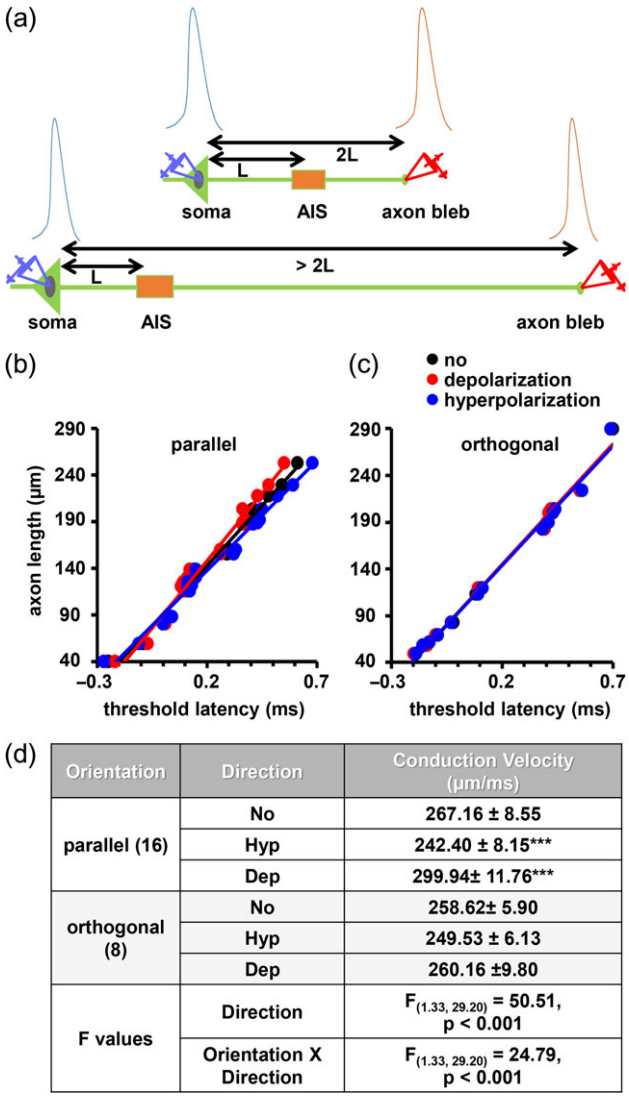

(d)

Orientation	Direction	Conduction Velocity (µm/ms)
parallel (16)	No	267.16 ± 8.55
	Hyp	242.40 ± 8.15***
	Dep	299.94± 11.76***
orthogonal (8)	No	258.62± 5.90
	Hyp	249.53 ± 6.13
	Dep	260.16 ±9.80
F values	Direction	$F_{(1.33, 29.20)} = 50.51$, $p < 0.001$
	Orientation X Direction	$F_{(1.33, 29.20)} = 24.79$, $p < 0.001$

Figure 3. Direct electric field alters the threshold latency and conduction velocity. Schematic of threshold latency measurement (*a*). If the distance from the soma to AIS is 'L' and the axon length is '2L', the AP generated in AIS takes a similar time to reach the soma and axon bleb (upper figure in *a*). However, when the axon is lengthier, the AP takes a longer time to arrive at the bleb than the soma (lower figure in *a*), this delay is the threshold latency. Threshold latency is linearly correlated to the axonal length in both parallel (*b*) (red, dep, $R^2 = 0.9787$; black, no, $R^2 = 0.9836$; blue, hyp, $R^2 = 0.984$) and orthogonal (*c*) (red, dep, $R^2 = 0.9915$; black, no, $R^2 = 0.9935$; blue, hyp, $R^2 = 0.9915$) field (parallel, $N = 19$, $n = 19$; orthogonal, $N = 15$, $n = 15$). The slope of the curve in figure (*b*) and (*c*) is AP conduction velocity, indexed for axons longer than 100 µm, in (*d*), values are mean ± SEM.

that polarization length increase during development (Fig. 1c), consistent with cortical layer-V pyramidal cell morphology changes along the first postnatal 4 weeks of brain development and maturation (Romand et al. 2011). For these reasons, our observations of maximal axon polarization length in neonatal mice (0.8 mm), which are already above any previous observations in soma or dendrites, may represent conservative estimates for the mature animal (human) case. A further source of underestimation is axon polarization length is expected to increase with distance from the soma (e.g., 1 mm) beyond the constraints of our experimental system (300 µm). Thus, conservatively, our data predict subthreshold modalities (such as tDCS and tACS) generate brain EF strength up to 0.5 V/m (Dmochowski et al. 2011; Minhas et al. 2012; Laakso et al. 2015) will polarize terminals >0.4 mV—making analog AP or synaptic modulation plausible. Suprathreshold modalities (such as DBS, TMS, and ECT) produce EFs > 60 V/m (McIntyre et al. 2004; Lopez-Quintero et al. 2010), leading to 48 mV axon polarization—well above axon AP threshold. Our results thus provide quantitative footing to long-held assumptions about axons as the cellular targets of neuromodulation. Effects on axons can complement those in dendritic compartments (Das et al. 2016; Kronberg et al. 2016; Lafon et al. 2016) where analog signal transduction is well established (Brunner and Szabadics 2016).

The heightened sensitivity of axons to electrical neuromodulation is presumed to derive from the electronic decoupling of the axon from the neuron trunk, with polarization length increased asymptotically with axon branch length up to a theoretical maximum polarization of $E\lambda$ (where λ is the passive space constant) (Arlotti et al. 2012). While we provide the first experimental evidence confirming this decoupling with distance, remarkably, the magnitude of polarization exceeded the maximum theoretically predicted for any passive model. Only a biophysical model with active conductance could explain heightened sensitivity, which is consistent with modulation of AP dynamics (Fig. 1h). Mechanistically, many of the same passive and active membrane properties that determine the excitability of terminals (blebs) during endogenous activity, including persistent Na^+ channels regulating gain modulation of neuronal input–output signaling (Crill 1996; Astman 2006), voltage-gated Na^+ channels controlling the neuronal excitability and signal conduction (Tian et al. 2014; Yin et al. 2015), HCN channels (Notomi and Shigemoto 2004; Benarroch 2013) or voltage-gated K^+ channel which attributes the AP broadening (Shu et al. 2006; Kole et al. 2007), may be engaged during exogenous electrical stimulation.

We provide the first direct evidence for axonal polarization under electrical stimulation, with comparatively minimal somatic polarization. Moreover, even weak terminal polarization was correlated with alterations of active intrinsic properties, such as AP kinetics (Fig. 2). This finding is in congruence with significant findings on analog–digital signal in the brain (Alle and Geiger 2006; Shu et al. 2006), where intracellular current injections at the soma alters AP morphology (Geiger and Jonas 2000; Shu et al. 2006; Kole et al. 2007; Debanne et al. 2013). Such AP kinetics alteration will subsequently affect synaptic efficacy (Shu et al. 2006) presumably because a broader AP arriving at the axon terminal induces a stronger calcium influx which potentiates the transmitter release thus resulting in a stronger synaptic current (Hori and Takahashi 2009). Whereas polarization induced by current injection at the soma fades along the axon, DCS-induced polarization increases along the axons maximizing towards the terminals, closer to the neurotransmitter release zone. Hence, in a chain of neurons, electrical stimulation could cause an incremental relay effect which may further enhance neuronal network activity. A canonical finding in subthreshold neuromodulation is altered synaptic efficacy (Jefferys 1981; Bikson et al. 2004; Rahman et al. 2013); this can be explained by our observed AP kinetics alterations that are correlated with the extent of terminal polarization (Fig. 2i,j).

Some clinical and cognitive outcomes of neuromodulation have been empirically linked to changes in sharp temporal tuning of intrahemispheric and interhemispheric connectivity (Hung et al. 2005; O'Shea et al. 2007; Polanía et al. 2011; Hartwigsen et al. 2013; Griffis et al. 2015), and our observations

of changes in conduction velocity may explain these changes. Alterations in AP conduction velocity may affect further circuit physiology. Beyond the analog value of each AP alone, depending on incoming axons orientations to a target neuron, temporal summations of spikes might be significantly altered. These may be substantial for spike-timing dependent plasticity, as the dendritic spike and synaptic event are on the order of a few milliseconds and determines the resultant potentiation or depression (Feldman 2012). Alterations in time of arrival in the excitatory or inhibitory drive may control postsynaptic spikes (Xue et al. 2014) and network oscillations (Buzsáki and Draguhn 2004). These further suggests a role in neuromodulation in signal synchrony. Hereby our findings provide direct evidence of analog–digital facilitation as a major result of neuromodulation.

Supplementary Material

Supplementary data is available at *Cerebral Cortex* online.

Authors' Contributions

D.C. performed the electrophysiological and D.Q.T. executed modeling experiments; D.C., M.B., and H.K. designed the experiments; D.C. and H.K. analyzed the data; M.B. and H.K. supervised the experiments; and M.B and H.K. secured the funding. All authors discussed results and interpretations and wrote the article.

Funding

Israel Science Foundation (grant number 287/15), the United States Department of Defense (grant number FA9550-13-1-0073), and the National Institutes of Health (grant numbers 1R01NS101362-01, 1R01MH111896-01, and 1R01NS095123-01).

Notes

The authors are grateful to Prof. Yousheng Shu for his valuable help in establishing the bleb patching technique. *Conflicts of Interest*: The authors declare that they have no conflicts of interest with the contents of this article.

References

Alle H, Geiger JRP. 2006. Combined analog and action potential coding in hippocampal mossy fibers. Science. 311:1290–1293.

Antal A, Ambrus GG, Chaieb L. 2014. The impact of electrical stimulation techniques on behavior. Wiley Interdiscip Rev Cogn Sci. 5:649–659.

Arlotti M, Rahman A, Minhas P, Bikson M. 2012. Axon terminal polarization induced by weak uniform DC electric fields: a modeling study. Conf Proc IEEE Eng Med Biol Soc. 2012: 4575–4578.

Astman N. 2006. Persistent sodium current in layer 5 neocortical neurons is primarily generated in the proximal axon. J Neurosci. 26:3465–3473.

Bahl A, Stemmler MB, Herz AVM, Roth A. 2012. Automated optimization of a reduced layer 5 pyramidal cell model based on experimental data. J Neurosci Methods. 210:22–34.

Benarroch EE. 2013. HCN channels: function and clinical implications. Neurology. 80:304–310.

Bikson M, Inoue M, Akiyama H, Deans JK, Fox JE, Miyakawa H, Jefferys JGR. 2004. Effects of uniform extracellular DC electric fields on excitability in rat hippocampal slices in vitro. J Physiol. 557:175–190.

Bischofberger J, Engel D, Li L, Geiger JRP, Jonas P. 2006. Patch-clamp recording from mossy fiber terminals in hippocampal slices. Nat Protoc. 1:2075–2081.

Brunner J, Szabadics J. 2016. Analogue modulation of back-propagating action potentials enables dendritic hybrid signalling. Nat Commun. 7:13033.

Buzsáki G, Draguhn A. 2004. Neuronal oscillations in cortical networks. Science. 304:1926–1929.

Clark B, Häusser M. 2006. Neural coding: hybrid analog and digital signalling in axons. Curr Biol. 16:R585–R588.

Crill WE. 1996. Persistent sodium current in mammalian central neurons. Annu Rev Physiol. 58:349–362.

Das S, Holland P, Frens MA, Donchin O. 2016. Impact of transcranial direct current stimulation (tDCS) on neuronal functions. Front Neurosci. 10:550.

Debanne D, Bialowas A, Rama S. 2013. What are the mechanisms for analogue and digital signalling in the brain? Nat Rev Neurosci. 14:63–69.

Debanne D, Campanac E, Bialowas A, Carlier E, Alcaraz G. 2011. Axon physiology. Physiol Rev. 91:555–602.

Dmochowski JP, Datta A, Bikson M, Su Y, Parra LC. 2011. Optimized multi-electrode stimulation increases focality and intensity at target. J Neural Eng. 8:46011.

Feldman DE. 2012. The spike-timing dependence of plasticity. Neuron. 75:556–571.

Fröhlich F, McCormick DA, Frohlich F, McCormick DA. 2010. Endogenous electric fields may guide neocortical network activity. Neuron. 67:129–143.

Geiger JR, Jonas P. 2000. Dynamic control of presynaptic Ca(2+) inflow by fast-inactivating K(+) channels in hippocampal mossy fiber boutons. Neuron. 28:927–939.

Griffis JC, Nenert R, Allendorfer JB, Szaflarski JP. 2015. Interhemispheric plasticity following intermittent theta burst stimulation in chronic poststroke aphasia. Neural Plast. 2016:20–23.

Hartwigsen G, Saur D, Price CJ, Ulmer S, Baumgaertner A, Siebner HR. 2013. Perturbation of the left inferior frontal gyrus triggers adaptive plasticity in the right homologous area during speech production. Proc Natl Acad Sci USA. 110: 16402–16407.

Hines ML, Carnevale NT. 1997. The NEURON simulation environment. Neural Comput. 9:1179–1209.

Holsheimer J. 2002. Which neuronal elements are activated directly by spinal cord stimulation. Neuromodulation. 5: 25–31.

Hori T, Takahashi T. 2009. Mechanisms underlying short-term modulation of transmitter release by presynaptic depolarization. J Physiol. 587:2987–3000.

Hu W, Shu Y. 2012. Axonal bleb recording. Neurosci Bull. 28: 342–350.

Hung J, Driver J, Walsh V. 2005. Visual selection and posterior parietal cortex: effects of repetitive transcranial magnetic stimulation on partial report analyzed by Bundesen's theory of visual attention. J Neurosci. 25:9602–9612.

Jefferys JG. 1981. Influence of electric fields on the excitability of granule cells in guinea-pig hippocampal slices. J Physiol. 319:143–152.

Kabakov AY, Muller PA, Pascual-Leone A, Jensen FE, Rotenberg A. 2012. Contribution of axonal orientation to pathway-dependent modulation of excitatory transmission by direct current stimulation in isolated rat hippocampus. J Neurophysiol. 107:1881–1889.

Kaphzan H, Buffington SA, Jung JI, Rasband MN, Klann E. 2011. Alterations in intrinsic membrane properties and the axon

initial segment in a mouse model of Angelman syndrome. J Neurosci. 31:17637–17648.

Kaphzan H, Buffington SA, Ramaraj AB, Lingrel JB, Rasband MN, Santini E, Klann E. 2013. Genetic reduction of the α1 subunit of Na/K-ATPase corrects multiple hippocampal phenotypes in Angelman syndrome. Cell Rep. 4:405–412.

Kole MH, Stuart GJ. 2008. Is action potential threshold lowest in the axon? Nat Neurosci. 11:1253–1255.

Kole MH, Stuart GJ. 2012. Signal processing in the axon initial segment. Neuron. 73:235–247.

Kole MHP, Letzkus JJ, Stuart GJ. 2007. Axon initial segment Kv1 channels control axonal action potential waveform and synaptic efficacy. Neuron. 55:633–647.

Kronberg G, Bridi M, Abel T, Bikson M, Parra LC. 2016. Direct current stimulation modulates LTP and LTD: activity dependence and dendritic effects. Brain Stimul. 10:51–58.

Laakso I, Tanaka S, Koyama S, De Santis V, Hirata A. 2015. Inter-subject variability in electric fields of motor cortical tDCS. Brain Stimul. 8:906–913.

Lafon B, Rahman A, Bikson M, Parra LC. 2016. Direct current stimulation alters neuronal input/output function direct current stimulation alters neuronal input/output function. Brain Stimul. 10:13–16.

Lopez-Quintero SV, Datta A, Amaya R, Elwassif M, Bikson M, Tarbell JM. 2010. DBS-relevant electric fields increase hydraulic conductivity of in vitro endothelial monolayers. J Neural Eng. 7:16005.

Márquez-Ruiz J, Leal-Campanario R, Sánchez-Campusano R, Molaee-Ardekani B, Wendling F, Miranda PC, Ruffini G, Gruart A, Delgado-García JM. 2012. Transcranial direct-current stimulation modulates synaptic mechanisms involved in associative learning in behaving rabbits. Proc Natl Acad Sci USA. 109:6710–6715.

McIntyre CC, Grill WM, Sherman DL, Thakor NV. 2004. Cellular effects of deep brain stimulation: model-based analysis of activation and inhibition. J Neurophysiol. 91:1457–1469.

Migliore M. 1996. Modeling the attenuation and failure of action potentials in the dendrites of hippocampal neurons. Biophys J. 71:2394–2403.

Minhas P, Bikson M, Woods AJ, Rosen AR, Kessler SK. 2012. Transcranial direct current stimulation in pediatric brain: a computational modeling study. Conf Proc IEEE Eng Med Biol Soc. 2012:859–862.

Notomi T, Shigemoto R. 2004. Immunohistochemical localization of Ih channel subunits, HCN1-4, in the rat brain. J Comp Neurol. 471:241–276.

Nowak LG, Bullier J. 1998. Axons, but not cell bodies, are activated by electrical stimulation in cortical gray matter. I. Evidence from chronaxie measurements. Exp Brain Res. 118: 477–488.

O'Shea J, Johansen-Berg H, Trief D, Göbel S, Rushworth MFS. 2007. Functionally specific reorganization in human premotor cortex. Neuron. 54:479–490.

Palmer LM, Stuart GJ. 2006. Site of action potential initiation in layer 5 pyramidal neurons. J Neurosci. 26:1854–1863.

Pashut T, Wolfus S, Friedman A, Lavidor M, Bar-Gad I, Yeshurun Y, Korngreen A. 2011. Mechanisms of magnetic stimulation of central nervous system neurons. PLoS Comput Biol. 7:e1002022.

Polanía R, Nitsche MA, Paulus W. 2011. Modulating functional connectivity patterns and topological functional organization of the human brain with transcranial direct current stimulation. Hum Brain Mapp. 32:1236–1249.

Purpura DP, McMurtry JG. 1965. Intracellular activities and evoked potential changes during polarization of motor cortex. J Neurophysiol. 28:166–185.

Radman T, Ramos RL, Brumberg JC, Bikson M. 2009. Role of cortical cell type and morphology in subthreshold and suprathreshold uniform electric field stimulation in vitro. Brain Stimul. 2:215–228.e3.

Rahman A, Reato D, Arlotti M, Gasca F, Datta A, Parra LC, Bikson M. 2013. Cellular effects of acute direct current stimulation: somatic and synaptic terminal effects. J Physiol. 591:2563–2578.

Ranck JB. 1975. Which elements are excited in electrical stimulation of mammalian central nervous system: a review. Brain Res. 98:417–440.

Rattay F. 1999. The basic mechanism for the electrical stimulation of the nervous system. Neuroscience. 89:335–346.

Romand S, Wang Y, Toledo-Rodriguez M, Markram H. 2011. Morphological development of thick-tufted layer v pyramidal cells in the rat somatosensory cortex. Front Neuroanat. 5:5.

Salvador R, Silva S, Basser PJ, Miranda PC. 2011. Determining which mechanisms lead to activation in the motor cortex: a modeling study of transcranial magnetic stimulation using realistic stimulus waveforms and sulcal geometry. Clin Neurophysiol. 122:748–758.

Shu Y, Duque A, Yu Y, Haider B, McCormick DA. 2007. Properties of action-potential initiation in neocortical pyramidal cells: evidence from whole cell axon recordings. J Neurophysiol. 97:746–760.

Shu Y, Hasenstaub A, Duque A, Yu Y, McCormick DA. 2006. Modulation of intracortical synaptic potentials by presynaptic somatic membrane potential. Nature. 441:761–765.

Strüber D, Rach S, Trautmann-Lengsfeld SA, Engel AK, Herrmann CS. 2014. Antiphasic 40 Hz oscillatory current stimulation affects bistable motion perception. Brain Topogr. 27:158–171.

Stuart GJ, Sakmann B. 1994. Active propagation of somatic action potentials into neocortical pyramidal cell dendrites. Nature. 367:69–72.

Tian C, Wang K, Ke W, Guo H, Shu Y. 2014. Molecular identity of axonal sodium channels in human cortical pyramidal cells. Front Cell Neurosci. 8:297.

Tranchina D, Nicholson C. 1986. A model for the polarization of neurons by extrinsically applied electric fields. Biophys J. 50: 1139–1156.

Xue M, Atallah BV, Scanziani M. 2014. Equalizing excitation–inhibition ratios across visual cortical neurons. Nature. 511: 596–600.

Yin L, Rasch MJ, He Q, Wu S, Dou F, Shu Y. 2015. Selective modulation of axonal sodium channel subtypes by 5-HT 1A receptor in cortical pyramidal neuron. Cereb Cortex. 27: 509–521.